Macromolecules
ARTICLE

Macromolecules **2010**, *43*, 9117–9125 **9117**
DOI: 10.1021/ma100765t

Effects of Solvent on the Phase Behavior of AB_n Miktoarm Star Copolymers

Ching-I Huang* and Li-Fan Yang

Institute of Polymer Science and Engineering, National Taiwan University Taipei 10617, Taiwan

Received April 12, 2010; Revised Manuscript Received September 9, 2010

ABSTRACT: We present a theoretical study of the effects of solvent on the phase behavior of AB_n miktoarm star copolymer solutions by adopting the self-consistent mean-field (SCMF) theory. In general, the associated effects with the addition of one solvent on the AB linear diblock copolymers hold true on the AB_n miktoarm star copolymers. However, due to the asymmetry of molecular architecture, AB_n exhibits a new spherical packing order of A15, which has to be considered in competition with the well-known body-centered cubic (BCC) and face-centered cubic (FCC) packing orders in the AB linear copolymer solutions. It is found that for A-formed spheres, the "normal" ones (i.e., formed when A is a minor block) can adopt two packing arrays of BCC and A15, while the "inverted" ones (i.e., formed when A is a major block) favor the A15 and FCC packing. Upon increasing the solvent amount/solvent selectivity, these A-formed inverted spheres tend to pack from BCC to FCC. Moreover, the transition of BCC/FCC → A15 with increasing the solvent selectivity is often induced by the fact that a greater degree of the interfacial distortion from a round into the polygonal shape in order to relax the stretching penalty for the B arms on the outside domains. On the other hand, as to the B-formed spheres, we do not observe any stable region of the A15 phase, but only BCC and FCC. This is mainly attributed to the tension of the highly stretched B within the inner domains, thus the AB interface tends to preserve a more spherical shape. In this case, we observe similar solvent effects on the stability of BCC and FCC packed spheres, as those in the AB linear diblock solutions.

I. Introduction

Due to its variant self-assembling behavior, block copolymers are widely applied in many nanotechnologies, such as photonic and biotechnological applications.[1,2] One of the major methods in controlling the morphological patterns is to dilute a block copolymer with solvents. Recently, with the improvement in synthetic techniques, copolymers with more complex forms of molecular architectures or with more than two types of monomers have been successfully formulated. This development leads to a rich variety of more fantastic morphologies, which may yield significant advances for block copolymers in novel technologies and applications. Thus, a greater understanding of how to control the phase behavior of copolymers with more complex architectures in both bulk and solution continues to be an attractive and important issue.

Miktoarm star copolymers, shown as in Figure 1, are one of the molecular architectures that have attracted a lot of attention. There have been some experimental[3−9] and theoretical[10−16] studies related to the morphological behavior in the melt. A systematic review of the theoretical results has been given by Grason.[15] Theoretically, Olvera de la Cruz et al.[10] were among the first to examine the stability criteria of microstructures formed by star copolymers. They found that a simple graft AB_2 copolymer is more difficult to microphase separately than a linear AB copolymer due to the greater change of entropy loss associated with the disorder-to-order transition. Milner et al.[11,12] applied the strong segregation theory (SST) to construct the phase diagram of A_mB_n miktoarm star copolymers in terms of the composition and the asymmetric parameter ε ($=(n_A/n_B)(l_A/l_B)^{1/2}$), where n_I and l_I are the number of arms and characteristic length of component I, respectively. The length parameter l_I is defined as $l_I = V_I/R_I^2$, where V_I and R_I correspond to the molecular volume and the radius of gyration of the respective blocks I. It is reported that at the same composition, varying the asymmetric parameter ε can trigger the evolvement of various microstructures. For instance, when the A composition $f = 0.5$, increasing the number of B arms in the AB_n miktoarm star copolymers is analogous to decreasing f, and thereafter a series of transition from lamellae (L) → gyroid of minority A (G_A) → hexagonally packed A-formed cylinders (C_A^{HEX}) → A-formed spheres (S_A) is expected. This is reasonable since the component with more arms experiences more lateral crowding and becomes more stretched; it tends to remain on the outside domains. Grason and Kamien[14] employed the self-consistent mean-field (SCMF) theory to construct the phase diagram of AB_n miktoarm star copolymers in terms of f and $\chi_{AB}N$ (χ_{AB} is the Flory−Huggins interaction parameter between components A and B, N is degree of copolymerization). Compared with AB linear diblock copolymers,

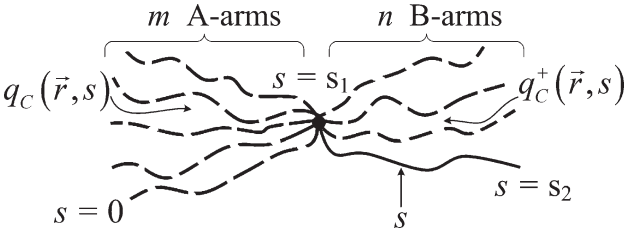

Figure 1. Schematic representation of the model A_mB_n miktoarm star copolymers. A length parameter along the copolymer chain, s, is defined starting from one of the free ends of A. $q_C(\vec{r},s)$ and $q_C^+(\vec{r},s)$ represent the end-integrated distribution function in a "forward" and "backward" diffusion pathway, respectively. When $s_1 < s < s_2$, $q_C(\vec{r},s)$ accounts for the probability that m A-arms and $n - 1$ B-arms have diffused to the junction point of $s = s_1$ (shown as the dashed lines), and then continues to diffuse along one B-arm (shown as the solid line) to the position $\vec{r}$ at s.

*To whom all correspondence should be addressed. Telephone: 886-2-33665886. Fax: 886-2-33665237. E-mail: chingih@ntu.edu.tw.

Published on Web 10/07/2010

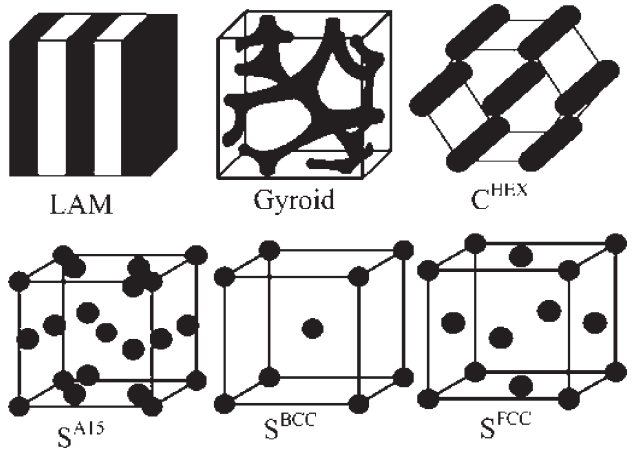

Figure 2. Schematic plot of all possible microstructures formed by the A_mB_n miktoarm star copolymers.

AB_n miktoarm star copolymers form similar ordered structures, such as lamellae (L), gyroid (G), hexagonally packed cylinders (C^{HEX}), and spheres (S), which are also mainly dominated by the composition. All possible microstructures formed by AB_n miktoarm star copolymers are schematically plotted in Figure 2. However, they discover two significant differences. First, the phase diagram is no longer symmetric about $f = 0.5$ and shifts toward $f > 0.5$. That is, the stability of microstructures with B blocks in the major domains is enhanced as the number of B arms n increases. This effect of molecular asymmetry on the shifting degree of the phase diagram reaches a limit when $n > 3$. Second, in addition to the commonly seen spherical packing order of body-centered cubic (BCC) arrays in block copolymers, a significantly stable regime of A15 packing array of A-formed spheres exists, illustrated as in Figure 2, between C_A^{HEX} and S_A^{BCC} in the AB_n miktoarm star copolymers. A simple way to manifest this fact is to treat each spherical ordered phase into the corresponding polyhedral Voronoi cell.[17,18] Generally speaking, there should be many ways for the copolymer chains to distribute and occupy the whole Voronoi lattice. One is to form a spherical AB interface, as frequently observed in the AB linear diblock copolymers. However, with an increase in the asymmetric degree of molecular architecture (i.e., increasing the number of B arms) and/or the composition of A, the AB interface tends to distort and reach the shape of the polyhedral Voronoi cell in order to relax the stretching penalty for the majority B-arms on the outside domains.[14] When considering the limited case that the AB interface adopts the same shape of the Voronoi cell, the minimization of free energy in the strong segregation limit leads to the stability of the A15 phase.[13] On the other hand, as the composition of A decreases, the A-formed minority domains become more spherical. Thus, they prefer to pack into the BCC lattice, which has been known as the most stable order for many soft spheres to minimize the cost of the chain stretching (overlapping) energy of the outer domains. Basically, these theoretical results are in good agreement with experimental results, except in the stability of spherical packing order.[3−9] Experimentally, neither the A15 nor the BCC lattice of spheres has been identified in melts of the miktoarm star copolymers. Indeed, Pochan et al.[3] reported that the spheres formed by polystyrene (PS)-polyisoprene $(PI)_2$ miktoarm star copolymers tend to be poorly ordered. It is hard to distinguish between each possible ordering (simple-cubic, BCC and A15, ...) from only a few weak peaks of small-angle X-ray scattering profiles. Though the A15 phase has not been identified in the miktoarm copolymers experimentally, it has been observed in other complex architectures, such as dendrimer[19−21] and amphiphilic surfactant[22−27] systems.

As many of the block copolymer systems with valuable technological applications involve the presence of solvents, the associated solvent effects on the morphological behavior need to be considered. In AB linear block copolymer solutions, a wealth of lyotropic and thermotropic order−order transitions (OOTs) and order−disorder transition (ODT) have been extensively studied. One of the significant results associated with the addition of one solvent is the formation of the so-called "inverted" phases, where the longer blocks form the minor domains. Upon increasing the solvent selectivity and/or solvent amount, the formed inverted spheres tend to pack from BCC into FCC. When considering the effects of solvent addition on the miktoarm copolymers, phase behavior becomes more complicated, since the A15 spherical phase has to be considered in competition with both BCC and FCC. Yet, a systematic examination of the effects of one solvent in transforming the melt phase behavior for miktoarm star copolymers has not been explored both experimentally and theoretically. Herein, we employ the SCMF theory to study the phase behavior of AB_n miktoarm star copolymer in the presence of a solvent. We adopt the Fourier space implementation of SCMF theory,[28] which can resolve the small differences of free energy between possible ordered phases. The model is formulated essentially by an extension of a multiply branched copolymer, which is constructed by Grason and Kamien,[14,29] in the presence of one solvent in a canonical ensemble. For simplicity, we restrict consideration to the phases of L, C^{HEX}, S^{A15}, S^{BCC}, and S^{FCC}, in order to construct the phase maps. Other possible complex phases such as the gyroid (G) and perforated layers (PL), which have been frequently observed between L and C^{HEX}, are not examined here. Moreover, we ignore the possibility of the disordered micellar regime as part of the disordered phase. That is, the disordered phase in our approach is simply the homogeneous state. We first choose the simplest architecture of miktoarm star copolymer, AB_2, as a model system, and systematically investigate how the morphological transition behavior is affected by solvent selectivity, copolymer volume fraction ϕ, and copolymer composition f. We then examine the effects of molecular asymmetry (i.e., number of multi-B arms n) on the formation of microstructures in the presence of a selective solvent. In addition to the ordered phases, the systems with lower values of copolymer volume fraction when the solvent selectivity is large may undergo a macrophase separation into two phases rich in the solvent and copolymer, respectively, which is, however, not our current concern. We thus use the Flory−Huggins thermodynamic analysis to locate the binodal coexistence curve between 2 disordered phases, for simplicity.[30] All the systems discussed later are chosen within the one ordered phase region.

II. Theory

We use a canonical ensemble approach and consider a monodisperse A_mB_n miktoarm star copolymer in the presence of a solvent S with average volume fractions ϕ and $1 - \phi$, respectively. The degree of copolymerization is N and A-monomer fraction in the copolymer is f. Each copolymer chain is composed of m identical arms of the A-block and n identical arms of the B-block at a common junction point (see Figure 1). Accordingly, each A-arm and B-arm has fN/m and $(1 - f)N/n$ monomers, respectively. We assume that the system is incompressible both locally and globally, and each monomer type has the same statistical segment length b. The local interaction between each pair of monomers I and J is quantified by the Flory−Huggins interaction parameter χ_{IJ}.

In general, the concentrations of A and B components at a given spatial position $\vec{r}$, $\phi_A(\vec{r})$ and $\phi_B(\vec{r})$, are attributed to the diffusion of each A and B monomer along the chains, respectively, into the spatial position $\vec{r}$. To consider the contribution

from the chain diffusion, we define a length parameter along the copolymer chain, s, so that there are $(\Delta s)N$ monomers within any chain interval of length Δs. We assume that each identical A-arm starts from $s = 0$ and terminates at the A−B junction point, $s = s_1$, and each identical B-arm ranges from $s = s_1$ to the free end, $s = s_2$. It is clear that $s_1 = f/m$ and $s_2 = f/m + (1-f)/n$. In order to solve the concentration profiles as well as the free energy in the equilibrium state, we begin with solving the copolymer partial partition functions, $q_C(\vec{r},s)$ and $q_C^+(\vec{r},s)$. We define $q_C(\vec{r},s)$ as the end-integrated distribution function, which is proportional to the probability that the chain portion of sN monomers diffuses from one of the free ends of the A-block, $s = 0$, to the spatial position $\vec{r}$ (referred as "forward" direction). While $q_C^+(\vec{r},s)$ computes the probability that the chain diffuses in the "backward" direction from one of the free ends of B-block, $s = s_2$, to the spatial position $\vec{r}$ at s. In further detail, when $0 < s < s_1$, $q_C(\vec{r},s)$ simply represents the probability that a single A-arm is diffused from the free end at $s = 0$ to $\vec{r}$ at s. But when $s_1 < s < s_2$, $q_C(\vec{r},s)$ accounts for the probability that m A-arms and $n-1$ B-arms have diffused from $s = 0$ and $s = s_2$, respectively, to the junction point of $s = s_1$, and then continues to diffuse along one B-arm to the spatial position $\vec{r}$ at s (see Figure 1). To summarize the above definition, $q_C(\vec{r},s)$ can be written as follows,

$$q_C(\vec{r},s) = \begin{cases} \int \mathrm{d}\vec{r}_\circ\, Q_C(\vec{r}_\circ,0;\vec{r},s) & \text{when } 0 < s < s_1 \\ \int \mathrm{d}\vec{r}_1\, Q_C(\vec{r}_1,s_1;\vec{r},s)[q_C(\vec{r}_1,s_1^-)]^m[q_C^+(\vec{r}_1,s_1^+)]^{n-1} & \text{when } s_1 < s < s_2 \end{cases} \tag{1}$$

where $Q_C(\vec{r}_i,s_i;\vec{r}_f,s_f)$ is the so-called chain propagator, which represents the distribution probability of the chain from monomer s_i at the spatial position $\vec{r}_i$ to monomer s_f at $\vec{r}_f$ in the presence of the external field $\omega(\vec{r})$. In eq 1 $q_C(\vec{r}_1, s_1^-)$ is the limit of the function as s approaches s_1 from the A-arm; while $q_C^+(\vec{r}_1, s_1^+)$ is computed by taking the limit $s \to s_1$ from the B-arm. Similarly, $q_C^+(\vec{r},s)$ can be expressed in the following equation:

$$q_C^+(\vec{r},s) = \begin{cases} \int \mathrm{d}\vec{r}_2\, Q_C(\vec{r}_2,s_2;\vec{r},s) & \text{when } s_1 < s < s_2 \\ \int \mathrm{d}\vec{r}_1\, Q_C(\vec{r}_1,s_1;\vec{r},s)[q(\vec{r}_1,s_1^-)]^{m-1}[q^+(\vec{r}_1,s_1^+)]^n & \text{when } 0 < s < s_1 \end{cases} \tag{2}$$

Because $q_C(\vec{r},s)$ and $q_C{}^+(\vec{r},s)$ are defined in terms of the chain propagator $Q_C(\vec{r}_i,s_i;\vec{r}_f,s_f)$, they satisfy the following modified diffusion equations:

$$\frac{\partial q_C(\vec{r},s)}{\partial s} = \begin{cases} \frac{1}{6}Nb^2\nabla^2 q_C(\vec{r},s) - \omega_A(\vec{r})q_C(\vec{r},s) & \text{if } 0 < s < s_1 \\ \frac{1}{6}Nb^2\nabla^2 q_C(\vec{r},s) - \omega_B(\vec{r})q_C(\vec{r},s) & \text{if } s_1 < s < s_2 \end{cases} \tag{3}$$

$$-\frac{\partial q_C^+(\vec{r},s)}{\partial s} = \begin{cases} \frac{1}{6}Nb^2\nabla^2 q_C^+(\vec{r},s) - \omega_A(\vec{r})q_C^+(\vec{r},s) & \text{if } 0 < s < s_1 \\ \frac{1}{6}Nb^2\nabla^2 q_C^+(\vec{r},s) - \omega_B(\vec{r})q_C^+(\vec{r},s) & \text{if } s_1 < s < s_2 \end{cases} \tag{4}$$

where $\omega_A(\vec{r})$ and $\omega_B(\vec{r})$ represent the external fields acting on the A segments and B segments along the copolymer chains, respectively. The boundary conditions for $q_C(\vec{r},s)$ and $q_C^+(\vec{r},s)$ are given by

$$\begin{aligned} q_C(\vec{r},0) &= 1 \\ q_C(\vec{r},s_1^+) &= [q_C(\vec{r},s_1^-)]^m[q_C^+(\vec{r},s_1^+)]^{n-1} \end{aligned} \tag{5}$$

$$\begin{aligned} q_C^+(\vec{r},s_2) &= 1 \\ q_C^+(\vec{r},s_1^-) &= [q_C(\vec{r},s_1^-)]^{m-1}[q_C^+(\vec{r},s_1^+)]^n \end{aligned} \tag{6}$$

The total partition function for a single miktoarm copolymer chain Q_C is found by integrating all possible configurations for the chains subject to the external fields and thus equal to

$$Q_C = \frac{1}{V}\int_V \mathrm{d}\vec{r}\, q_C(\vec{r},s = s_2) \tag{7}$$

For the solvent particles, we adopt the previously established formalism in the AB linear block copolymer solutions.[31] The partition function Q_S subject to the field $_S(\vec{r})$ is simply equal to

$$Q_S = \frac{1}{V}\int_V \mathrm{d}\vec{r}\, \exp\left[\frac{-\omega_S(\vec{r})}{N}\right] \tag{8}$$

which indeed can be rewritten as

$$Q_S = \frac{1}{V}\int_V \mathrm{d}\vec{r}\, q_S\left(\vec{r},s = \frac{1}{N}\right) \tag{9}$$

where $q_S(\vec{r},s)$ satisfies

$$\frac{\partial q_S(\vec{r},s)}{\partial s} = -\omega_S(\vec{r})q_S(\vec{r},s) \tag{10}$$

with the initial condition $q_s(\vec{r},s = 0) = 1$.

For arbitrary volume fraction profiles of each component, $\phi_I(\vec{r})$; I = A, B, S, which depend on the segment distribution functions subject to the external fields $\omega_I(\vec{r})$; I = A, B, S, the free energy per molecule F is given by[28]

$$\begin{aligned} \frac{F}{k_BT} &= -\phi\ln\left[\frac{Q_C}{\phi}\right] - (1-\phi)N\ln\left[\frac{Q_S}{1-\phi}\right] \\ &- \frac{1}{V}\int_V \mathrm{d}\vec{r}\,[\omega_A(\vec{r})\phi_A(\vec{r}) + \omega_B(\vec{r})\phi_B(\vec{r}) + \omega_S(\vec{r})\phi_S(\vec{r})] \\ &+ \frac{1}{V}\int_V \mathrm{d}\vec{r}\,[\chi_{AB}N\phi_A(\vec{r})\phi_B(\vec{r}) + \chi_{AS}N\phi_A(\vec{r})\phi_S(\vec{r}) \\ &+ \chi_{BS}N\phi_B(\vec{r})\phi_S(\vec{r})] + \frac{1}{V}\int_V \mathrm{d}\vec{r}\,\eta(\vec{r})[\phi_A(\vec{r}) + \phi_B(\vec{r}) + \phi_S(\vec{r}) - 1] \end{aligned} \tag{11}$$

where $\eta(\vec{r})$ is the effective pressure field to ensure the local incompressibility of the system. On the basis of the minimization of the free energy in eq 11 with respect to $\phi_I(\vec{r})$ and $\omega_I(\vec{r})$; I = A, B, S, the external fields and the volume fraction profiles have to satisfy

$$\begin{aligned} \omega_A(\vec{r}) - \omega_S(\vec{r}) &= \chi_{AB}N\phi_B(\vec{r}) + \chi_{AS}N\phi_S(\vec{r}) \\ &- \chi_{AS}N\phi_A(\vec{r}) - \chi_{BS}N\phi_B(\vec{r}) \end{aligned}$$

$$\begin{aligned} \omega_B(\vec{r}) - \omega_S(\vec{r}) &= \chi_{AB}N\phi_A(\vec{r}) + \chi_{BS}N\phi_S(\vec{r}) \\ &- \chi_{AS}N\phi_A(\vec{r}) - \chi_{BS}N\phi_B(\vec{r}) \end{aligned}$$

$$\phi_A(\vec{r}) = \frac{\phi m}{Q_C}\int_0^{s_1} ds\, q_C(\vec{r},s)q_C^+(\vec{r},s)$$

$$\phi_B(\vec{r}) = \frac{\phi n}{Q_C}\int_{s_1}^{s_2} ds\, q_C(\vec{r},s)q_C^+(\vec{r},s)$$

$$\phi_S(\vec{r}) = \frac{1-\phi}{Q_S}\exp\left[\frac{-\omega_S(\vec{r})}{N}\right] = \frac{1-\phi}{Q_S}\, q_S(\vec{r}, s = 1/N)$$

$$\phi_A(\vec{r}) + \phi_B(\vec{r}) + \phi_S(\vec{r}) = 1 \tag{12}$$

For a disordered state, the volume fractions $\phi_I(\vec{r})$ and the fields $\omega_I(\vec{r})$ are constants, I = A, B, S. The partition functions are simply $Q_C = \exp(-f\omega_A - (1-f)\omega_B)$ and $Q_S = \exp(-\omega_S/N)$. As a result, eq 11 is reduced to the Flory−Huggins mean-field free energy functional per molecule in the disordered state, i.e.

$$\frac{F}{k_B T}_{disorder} = \phi\ln\phi + (1-\phi)N\ln(1-\phi) + f(1-f)\chi_{AB}N\phi^2 + f\chi_{AS}N\phi(1-\phi) + (1-f)\chi_{BS}N\phi(1-\phi) \tag{13}$$

As only one characteristic size is involved with the periodic morphologies concerned here, it is most efficient to perform the SCMF calculations using the Fourier-space algorithm. That is, any given function, $g(\vec{r})$, is expressed in terms of the corresponding amplitudes, g_j, with respect to a series of orthonormal basis function $f_j(\vec{r})$

$$g(\vec{r}) = \sum_j g_j f_j(\vec{r})$$

The basis functions reflect the symmetry of the ordered phase being considered and are selected to be eigenfunctions of the Laplacian operator

$$\nabla^2 f_j(\vec{r}) = -\lambda_j L^{-2} f_j(\vec{r}) \tag{14}$$

where L is the lattice spacing for the ordered phase. The basis functions are ordered to start with $f_1(\vec{r}) = 1$ such that λ_j is an increasing series. For lamellae $f_j(x) = 2^{1/2}\cos(2\pi(j-1)x/L)$, $j \geq 2$, where x is the coordinate orthogonal to the lamellae. Basis functions for the phases with other space-group symmetries can be found in ref 32. Note that the number of basis functions varies with the ordered phase and the segregation degree. In any case, the sufficient number of basis functions has to be included in our computations in order to ensure that the results reach the equilibrium values.

Next, we give the resultant Fourier-space implementation of the SCMF calculations. When the amplitudes corresponding to the basis functions are utilized, eqs 3, 4, and 10 for solving $q_C(\vec{r},s)$, $q_C^+(\vec{r},s)$, and $q_S(\vec{r},s)$ become

$$\frac{dq_{C,i}}{ds} = \begin{cases} \sum_j A_{ij}q_{C,j} & \text{if } 0 < s < s_1 \\ \sum_j B_{ij}q_{C,j} & \text{if } s_1 < s < s_2 \end{cases} \quad i = 1,2,3,\ldots \tag{15}$$

$$\frac{dq_{C,i}^+}{ds} = \begin{cases} -\sum_j A_{ij}q_{C,j}^+ & \text{if } 0 < s < s_1 \\ -\sum_j B_{ij}q_{C,j}^+ & \text{if } s_1 < s < s_2 \end{cases} \quad i = 1,2,3,\ldots \tag{16}$$

$$\frac{dq_{S,i}}{ds} = \sum_j C_{ij}q_{S,j} \quad i = 1,2,3,\ldots \tag{17}$$

The matrices A_{ij}, B_{ij}, and C_{ij} are given by

$$A_{ij} = -\frac{Nb^2}{6L^2}\lambda_i\delta_{ij} - \sum_k \omega_{A,k}\Gamma_{ijk}$$

$$B_{ij} = -\frac{Nb^2}{6L^2}\lambda_i\delta_{ij} - \sum_k \omega_{B,k}\Gamma_{ijk}$$

$$C_{ij} = -\sum_k \omega_{S,k}\Gamma_{ijk} \tag{18}$$

with

$$\Gamma_{ijk} = \frac{1}{V}\int_V d\vec{r}\, f_i(\vec{r})f_j(\vec{r})f_k(\vec{r})$$

$\omega_{A,k}$, $\omega_{B,k}$, and $\omega_{S,k}$ are the corresponding amplitudes with respect to the kth basis function for fields $\omega_A(\vec{r})$, $\omega_B(\vec{r})$, and $\omega_S(\vec{r})$, respectively. The initial conditions for solving eqs 15−17 are $q_{C,i}(s=0) = \delta_{i1}$, $q_{C,i}^+(s=s_2) = \delta_{i1}$, and $q_{S,i}(s=0) = \delta_{i1}$. In addition, the corresponding amplitude with respect to the ith basis function for $q_C(\vec{r},s)$ and $q_C^+(\vec{r},s)$ at the junction point of $s = s_1$ is determined by

$$\begin{aligned} q_{C,i}(s_1^+) &= \frac{1}{V}\int_V d\vec{r}\,[q_C(\vec{r},s_1^-)]^m[q_C^+(\vec{r},s_1^+)]^{n-1}f_i(\vec{r}) \\ q_{C,i}^+(s_1^-) &= \frac{1}{V}\int_V d\vec{r}\,[q_C(\vec{r},s_1^-)]^{m-1}[q_C^+(\vec{r},s_1^+)]^n f_i(\vec{r}) \end{aligned} \tag{19}$$

Once the amplitudes of $q_C(\vec{r},s)$, $q_C^+(\vec{r},s)$, and $q_S(\vec{r},s)$ are solved, the amplitudes of the volume fraction profiles and external fields of each component can be obtained as follows

$$\phi_{A,i} = \frac{m\phi}{q_{C,1}(s_2)}\sum_{j,k}\Gamma_{ijk}\int_0^{s_1} ds\, q_{C,j}(s)q_{C,k}^+(s)$$

$$\phi_{B,i} = \frac{n\phi}{q_{C,1}(s_2)}\sum_{j,k}\Gamma_{ijk}\int_{s_1}^{s_2} ds\, q_{C,j}(s)q_{C,k}^+(s)$$

$$\phi_{S,i} = \frac{1-\phi}{q_{S,1}(1/N)}\, q_{s,i}\left(\frac{1}{N}\right)$$

$$\phi_{A,i} + \phi_{B,i} + \phi_{S,i} = \delta_{i1}$$

$$\begin{aligned} \omega_{A,i} - \omega_{S,i} &= \chi_{AB}N\phi_{B,i} + \chi_{AS}N\phi_{S,i} - \chi_{AS}N\phi_{A,i} - \chi_{BS}N\phi_{B,i} \\ \omega_{B,i} - \omega_{S,i} &= \chi_{AB}N\phi_{A,i} + \chi_{BS}N\phi_{S,i} - \chi_{AS}N\phi_{A,i} - \chi_{BS}N\phi_{B,i} \end{aligned} \tag{20}$$

The free energy per molecule F is thus given by

$$\begin{aligned} \frac{F}{k_B T} = &-\phi\ln\left[\frac{q_{C,1}(s_2)}{\phi}\right] - (1-\phi)\mathrm{N}\ln\left[\frac{q_{S,1}(1/\mathrm{N})}{1-\phi}\right] \\ &- \sum_i(\omega_{A,i}\phi_{A,i} + \omega_{B,i}\phi_{B,i} + \omega_{S,i}\phi_{S,i}) \\ &+ \sum_i(\chi_{AB}N\phi_{A,i}\phi_{B,i} + \chi_{AS}N\phi_{A,i}\phi_{S,i} + \chi_{BS}N\phi_{B,i}\phi_{S,i}) \end{aligned} \tag{21}$$

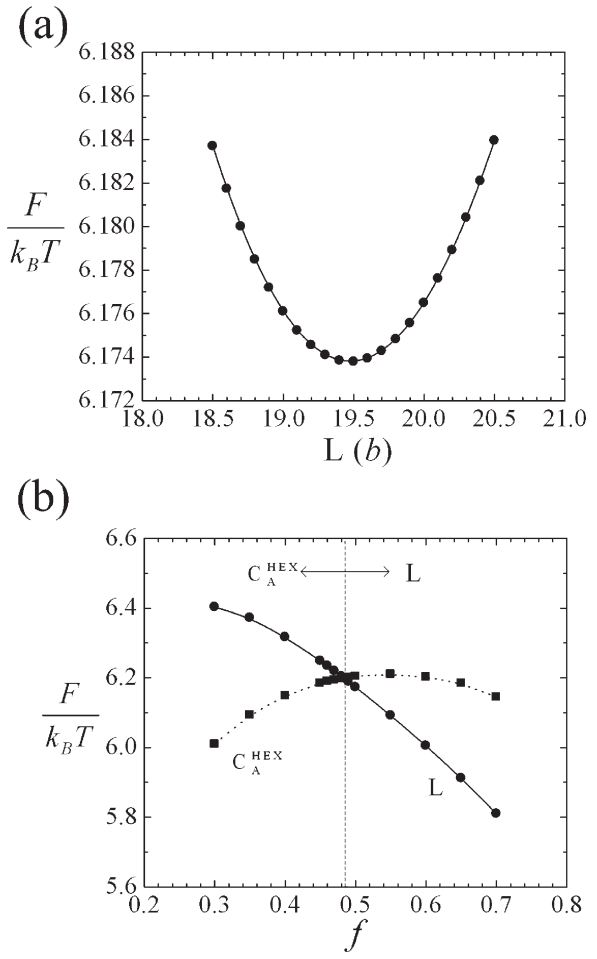

Figure 3. (a) Plot of the free energy term in eq 21 versus the lattice spacing L for an AB_2 miktoarm copolymer melt to form a lamellar phase at $f = 0.5$, $N = 150$, and $\chi_{AB}N = 40$. (b) Comparison of the free energy between lamellae (L) and hexagonally packed A-formed spheres (C_A^{HEX}) at various values of composition f for AB_2 copolymer melt when $N = 150$ and $\chi_{AB}N = 40$.

For a periodic ordered phase, the free energy has to be minimized with respect to the lattice spacing L. For example, in Figure 3a we show a typical plot of the free energy term in eq 21 versus the lattice spacing L when an AB_2 miktoarm copolymer melt is assumed to form a lamellar phase at $f = 0.5$, $N = 150$, and $\chi_{AB}N = 40$. Similarly, the minimum values of the free energy with respect to the lattice spacing L for other possible phases can be obtained. Then, to determine the most stable phase one has to compare free energies of possible phases. In Figure 3b we compare the free energies of two typical ordered phases of L and C_A^{HEX} as an example to determine the most stable phase at various values of composition f for AB_2 copolymer melt when $N = 150$ and $\chi_{AB}N = 40$. It is clear that the phase boundary between L and C_A^{HEX} occurs at $f = 0.485$.

III. Results and Discussion

In order to examine the solution phase behavior of AB_n miktoarm star copolymers, we first choose AB_2 with $N = 150$ and $\chi_{AB}N = 40$ in the presence of a B-selective solvent S with the interaction parameters χ_{AS}=0.7 and χ_{BS}=0.4. Figure 4 presents the corresponding phase map in terms of f and ϕ. As expected, when the solutions are concentrated, the formation of equilibrium morphology is mainly dominated by the composition f, similar to that in the AB_2 copolymer melt.[14]

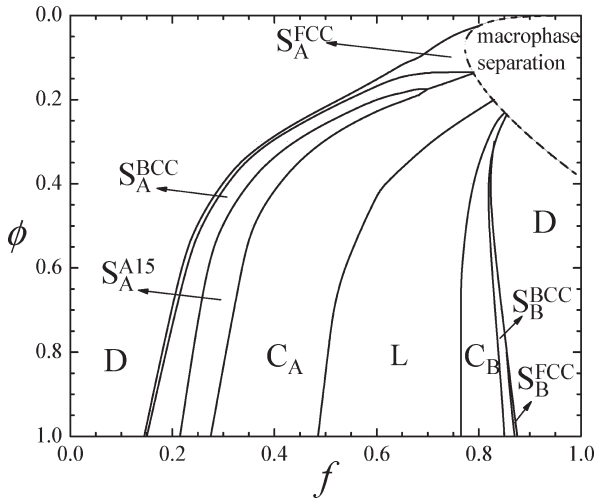

Figure 4. Two-dimensional phase map as a function of f and ϕ for an AB_2 star copolymer solution with $N = 150$, $\chi_{AB}N = 40$, $\chi_{AS} = 0.7$, and $\chi_{BS} = 40$.

As the solutions become less concentrated, due to the fact that the S solvent prefers the B block and acts in a manner that corresponds qualitatively to reducing the A composition, the formation of A-formed cylinders as well as spheres is expected even for $f > 0.5$. It is interesting to find that a region of S^{FCC} always occurs near the ODT in the phase diagram. When f is small, this ordered S_A^{FCC} regime is very narrow, as observed in both the AB linear and AB_n miktoarm copolymer melts. When considering the disordered micellar structure as part of the disordered phase, the FCC packing is likely to disappear in the copolymer melts.[33,34] Accordingly, as it has been discussed in the AB_n miktoarm copolymer melt, a spherical ordering of BCC or A15 is favored over FCC when the minority block forms the spheres in the solutions. However, as f increases to ≥0.5 so that the majority A blocks form the spheres when ϕ is small, the corona layers become thinner with increasing f. This enables the spheres to adopt a more dense packing order such as FCC. Thus, we observe a significant expansion of the ordered S_A^{FCC} regime near the ODT with an increase in the composition of unfavorable A blocks f (Figure 4). Furthermore, the stable S_A^{BCC} and S_A^{A15} regions are reduced and even disappear with an increase in f, indicating that the so-called inverted spheres formed by the majority blocks (i.e., with smaller corona layers) prefer a more dense FCC over a BCC or A15 packing. Note that due to the immiscibility between A block and solvent, a macrophase separation into an AB_n copolymer-rich phase and a S-rich phase occurs when $f > 0.5$ and $\psi < 1$. For simplicity, we use the Flory–Huggins thermodynamic analysis to locate the binodal coexistence curve between 2 disordered AB_n-rich and S-rich phases.

Next we would like to examine the effects of solvent selectivity and solvent amount on the microstructure formation of AB_n miktoarm star copolymers. For this purpose, two types of A-selective and B-selective solvents are respectively added into the AB_2 copolymer with $f < 0.5$ and $f > 0.5$, respectively. Accordingly, there are four possible types of microstructures, A-formed normal, A-formed inverted, B-formed normal, and B-formed inverted structures. We first choose an AB_2 with $f = 0.25$ and $N = 150$ so that the minority A component forms the spheres, which adopts a BCC ($21.9 < \chi_{AB}N < 26.2$) and then A15 packing order ($\chi_{AB}N > 26.2$). By adding a B-selective solvent ($\chi_{AS} \geq \chi_{BS} = 0.4$), we can see how the packing order of these A-formed normal spheres is affected. Parts a–c of Figure 5 display the two-dimensional phase maps in terms of $\chi_{AB}N$ and ϕ when $\chi_{AS} = 0.4$, 0.7, and 0.75, respectively. As it is shown in Figure 5a, when a neutral and good solvent ($\chi_{AS} = \chi_{BS} = 0.4$) is

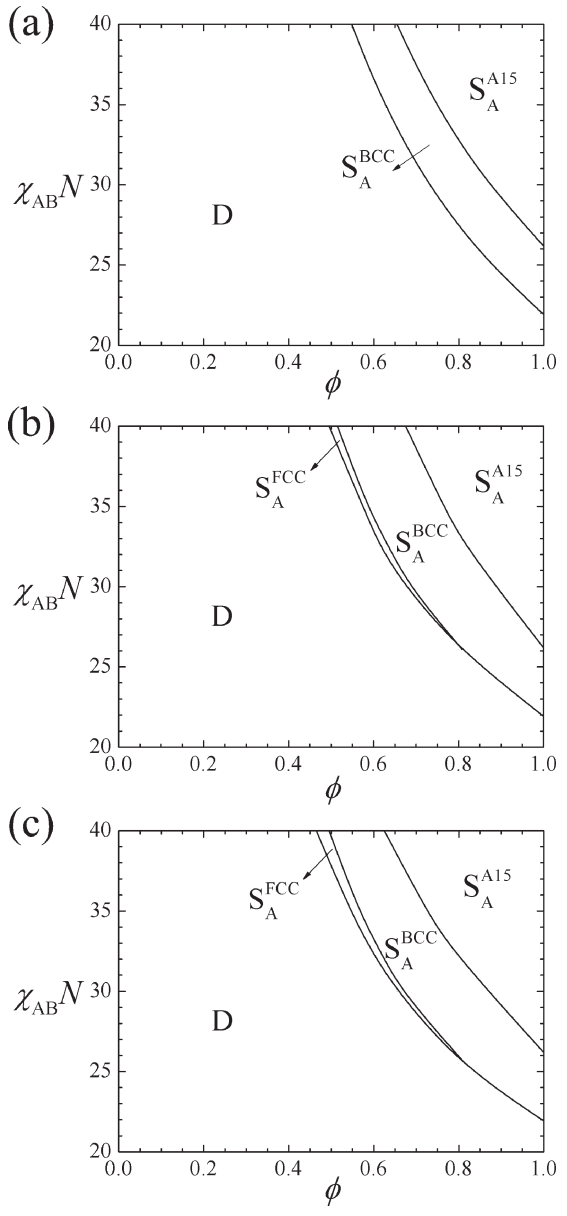

Figure 5. Two-dimensional phase map in terms of ϕ and $\chi_{AB}N$ for an AB_2 star copolymer solution with $f = 0.25$ and $N = 150$ at a fixed value of $\chi_{BS} = 0.4$ and χ_{AS} = (a) 0.4, (b) 0.7, and (c) 0.75, respectively.

added to this asymmetric copolymer at $\chi_{AB}N > 26.2$, a sequential lyotropic transition from $S_A^{A15} \rightarrow S_A^{BCC} (\rightarrow S_A^{FCC}) \rightarrow D$ is observed. Based on the fact that the incompatibility between the A and B blocks is reduced by the presence of a neutral and good solvent, this lyotropic transition is analogous to the thermotropic transition by decreasing the $\chi_{AB}N$ value in the melt phase map at a fixed $f = 0.25$. When the solvent S becomes B-selective, since it prefers the B blocks and thus expected to partition into the B-rich domains, the same transition trend as that in the melt by decreasing the f composition from $S_A^{A15} \rightarrow S_A^{BCC} (\rightarrow S_A^{FCC}) \rightarrow D$ is also expected. When the selectivity of the added solvent increases to $\chi_{AS} = 0.7$ (Figure 5b) or 0.75 (Figure 5c), we observe that though each ordered regime is enlarged slightly, the phase transitions are similar to those in the neutral solutions.

In examining the solvent effects on the formation of A-formed inverted structures, we choose an AB_2 with $f = 0.6$ in the presence of a B-selective solvent S. In particular, we set χ_{BS} equal to 0.4 and vary $\chi_{AS} \geq 0.4$. Figure 6 displays the resultant phase map as a function of χ_{AS} and ϕ for AB_2 copolymer with $f = 0.6$ and

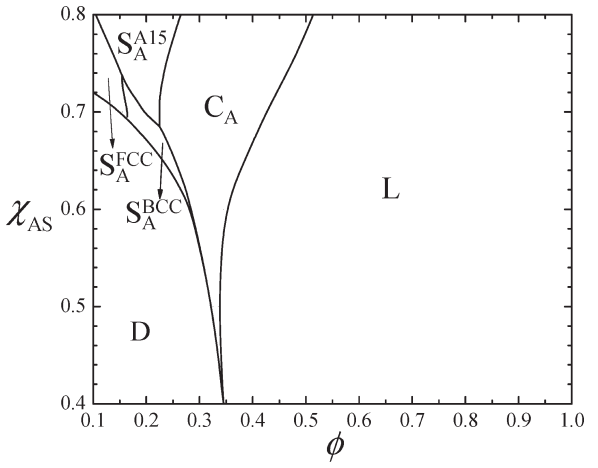

Figure 6. Two-dimensional phase map as a function of ϕ and χ_{AS} for an AB_2 star copolymer solution with $f = 0.6$, $N = 150$, $\chi_{BS} = 0.4$, and $\chi_{AB}N = 40$.

$N = 150$ at $\chi_{AB}N$ equal to 40. As it is expected, upon dilution by adding a B-selective solvent (i.e., decreasing ϕ), a sequence from $L \rightarrow C_A^{HEX} \rightarrow S_A \rightarrow D$ is observed. More interestingly, the packing order of A-formed spheres is dependent on the solvent selectivity. When the selectivity of the added solvent for B is not significant enough (such as $\chi_{AS} < 0.68$ here), these A-formed spheres prefer the BCC packing. But, they tend to move toward into A15 or FCC array with increasing the solvent selectivity and/or dilution. The transition mechanism of $S^{BCC} \rightarrow S^{FCC}$ induced by increasing the solvent amount/solvent selectivity has been proposed in the AB linear block copolymer solutions.[30,35] Previously, we have theoretically shown that for the spheres formed in the slightly selective solvent, though the solvent partitions preferentially to the matrix domains, there still remains a considerable amount of solvent inside the cores.[30] Furthermore, not 100% copolymer chains aggregate to form the micelles. Consequently, the intermicellar interactions become softer and thus these spheres adopt a BCC array. Upon increasing the solvent selectivity, though more solvents are expelled from the core which may cause a decrease in the micellar diameter, the fact that more free chains remaining in the matrix are driven to aggregate into the spheres enables an increase in the spherical diameter. As a result, these formed spheres become more impenetrable and adopt a FCC lattice. In further, the increase in segregation to minimize the unfavorable A−S interactions enables a decrease in the interfacial width between domains and consequently the area per chain. This requires an increase in chain stretching normal to the interface, resulting in an increase in the size of the matrix domains. When extended to the case of AB_n copolymer solutions, one should consider that when more chains aggregate to form cylinders or micelles upon increasing the solvent selectivity, this chain stretching penalty for the B-arms on the matrix domains becomes more significant. Thus, a greater degree of the interfacial distortion from a round into a polygonal shape is accompanied in order to relax the stretching penalty for the B multiarms on the outside domains. As it can be seen clearly in Figure 7a, where we display the corresponding spherical patterns when χ_{AS} varies from 0.69 (S_A^{BCC}) to 0.8 (S_A^{A15}) for AB_2 copolymer solutions with $f = 0.6$, $N = 150$, $\chi_{AB}N = 40$, $\chi_{BS} = 0.4$, and $\phi = 0.2$, all the A-formed spheres are round-like when they pack into a BCC ordering, but they become oblate-like on the faces of the $Pm\bar{3}n$ unit cell when they pack into an A15 array. Each oblate spheroid is characteristic of the equatorial diameter b larger than the polar diameter c, as it is shown in Figure 7a. Here we define the interfacial shape parameter α as the ratio b/c to quantify the degree of the distortion of the AB interface. Figure 7b plots the

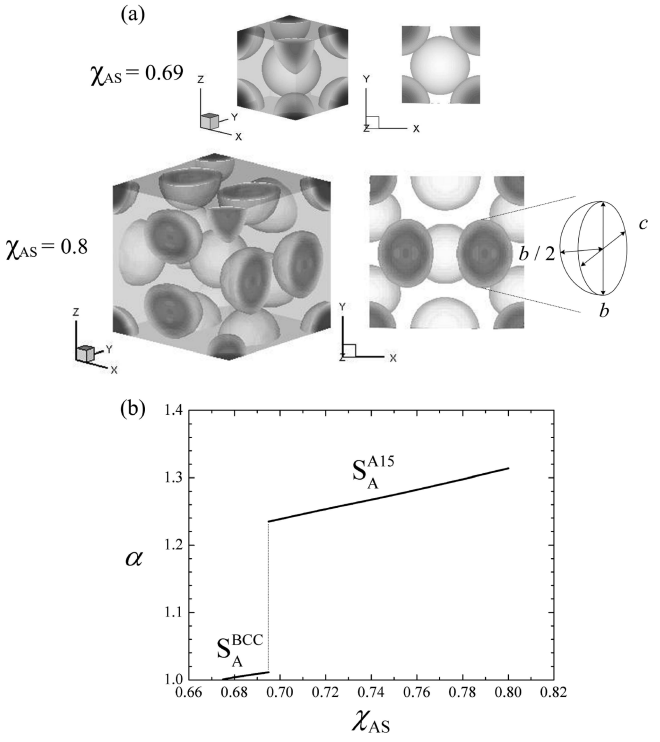

Figure 7. (a) Density plots of the A-formed spherical patterns in a BCC and A15 ordering, respectively, for an AB_2 star copolymer solution with $f = 0.6$, $N = 150$, $\phi = 0.2$, $\chi_{AB}N = 40$, $\chi_{BS} = 0.4$, and χ_{AS} equal to 0.69 and 0.8, respectively. (b) Variation of the interfacial shape parameter α with χ_{AS} for the solutions as in part a.

corresponding value of α as a function of χ_{AS} for the solutions in Figure 7a. As expected, with increasing the solvent selectivity (χ_{AS}), the interfacial shape parameter α is very close to 1.0 in the S_A^{BCC} ordered phase; it then significantly jumps to a larger value and keeps increasing in the S_A^{A15} phase. On the basis of the fact that the AB interface experiences a greater degree of distortion into the polygonal Voronoi cell upon increasing the solvent selectivity for the B multiarms on the matrix domains, it is reasonable to observe that both the C_A^{HEX} and S_A^{A15} ordered regimes are greatly enlarged with χ_{AS}.

If we choose the same AB_2 copolymer system as in Figure 6 ($f = 0.6$, $N = 150$, and $\chi_{AB}N = 40$) but in the presence of an A-selective solvent ($\chi_{BS} > \chi_{AS} = 0.4$), the resultant microstructures are thus formed by the minority B-arms, i.e., B-formed normal structures. As it is shown in Figure 8, where we display the corresponding phase map as a function of χ_{BS} and ϕ, a transition of L → C_B^{HEX} → S_B → D occurs with increasing dilution. Due to the fact that the multi B-arms experience more lateral crowding than the linear A block, they need more space to get stretched and thus hard to be confined within the minor domains. Hence, we observe a significantly large region of the ordered lamellae. Moreover, when the B-arms curl to form the spheres, the tension of the highly stretched inner domains prefers a more spherical interface than a polygonal interface. Accordingly, the A15 phase is not stable here. The fact that these B-formed normal spheres prefer the BCC packing and move toward into a FCC array with increasing the solvent selectivity and/or dilution is simply attributed to the same solvent effects as in the AB linear block copolymer systems. Even when the copolymer composition f decreases to <0.5 so that the corona layers for these B-formed inverted spheres become thinner, we still do not find any stable region of the A15 phase. Only the FCC packing is observed. As it is displayed in Figure 9, where we plot the phase map as a function of χ_{BS} ($\chi_{AS} = 0.4$) and ϕ for AB_2 copolymer with $f = 0.4$ and

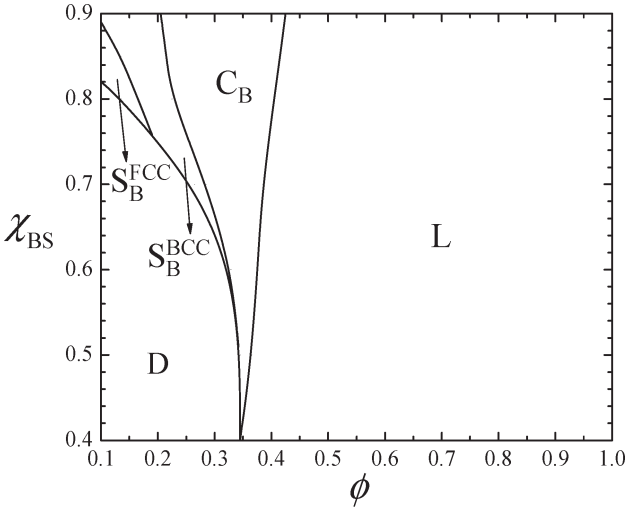

Figure 8. Two-dimensional phase map as a function of ϕ and χ_{BS} for an AB_2 star copolymer solution with $f = 0.6$, $N = 150$, $\chi_{AB}N = 40$, and $\chi_{AS} = 0.4$.

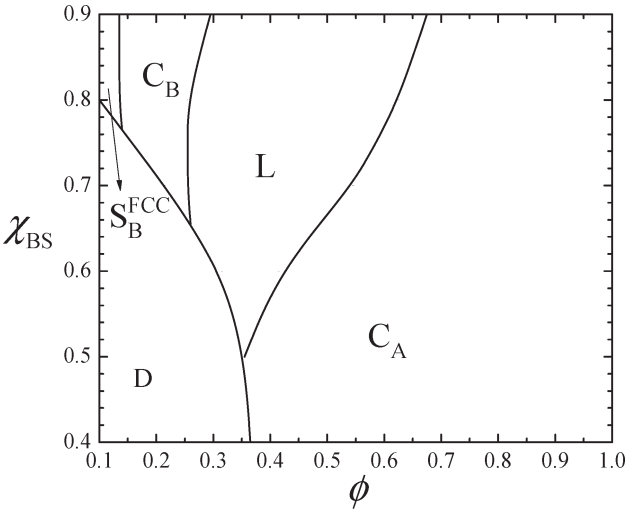

Figure 9. Two-dimensional phase map as a function of ϕ and χ_{BS} for an AB_2 star copolymer solution with $f = 0.4$, $N = 150$, $\chi_{AB}N = 40$, $\chi_{AS} = 0.4$.

$N = 150$ at $\chi_{AB}N$ equal to 40, a sequential transition of C_A^{HEX} → L → C_B^{HEX} → S_B^{FCC} → D occurs upon dilution.

So far, with the simplest miktoarm copolymer of AB_2 as a model system, we have illustrated the significant effects of solvent addition on the resultant morphological behavior. Now, we extend our study to AB_n copolymers, and investigate whether the formed microstructure type is strongly dependent on the number of B arms, n, at the same composition f and degree of copolymerization N. Here we also include the results for AB linear diblock copolymer ($n = 1$) as a comparison. Figure 10a presents the two-dimensional phase map in terms of n and ϕ for an AB_n copolymer with $f = 0.25$ and $N = 150$ at $\chi_{AB}N$ equal to 40 in the presence of a B-selective solvent by setting $\chi_{BS} = 0.4$ and $\chi_{AS} = 0.7$. It is clear that in the concentrated regime when n varies from 1 to ≥2, the ordered region of C_A^{HEX} is replaced by S_A^{A15}. This reflects the fact that the presence of the component with more arms (B) on the outside domains is enhanced when the molecules vary from a linear to an asymmetric miktoarm architecture; moreover, the AB interface tends to distort and reach the polyhedral shape in order to relax the stretching penalty for the multi B-arms. When $n \geq 2$, the same lyotropic transition from S_A^{A15} → S_A^{BCC} → S_A^{FCC} → D occurs, as we have explained in

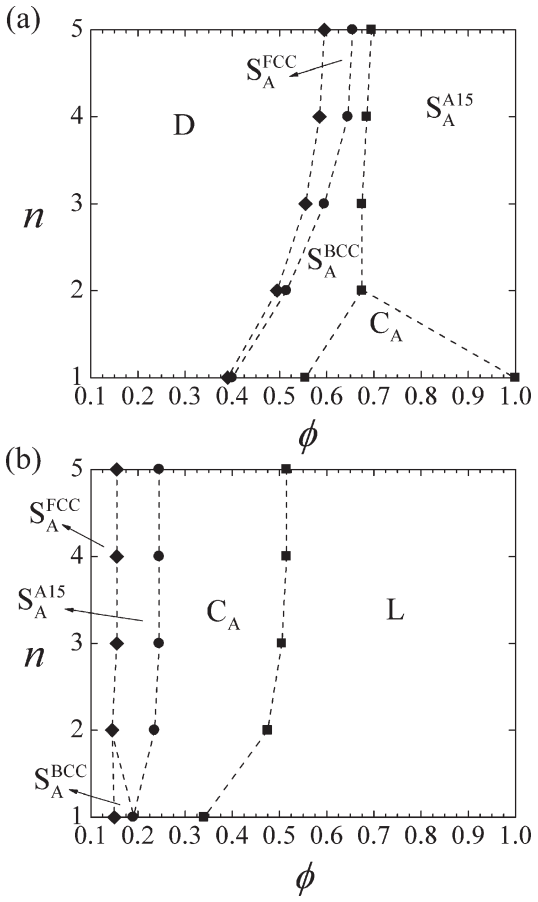

Figure 10. Two-dimensional phase maps in terms of ϕ and n for AB_n star copolymer solutions with $N = 150$, $\chi_{AB}N = 40$, $\chi_{BS} = 0.4$, and (a) $f = 0.25$, $\chi_{AS} = 0.7$, (b) $f = 0.6$, $\chi_{AS} = 0.75$.

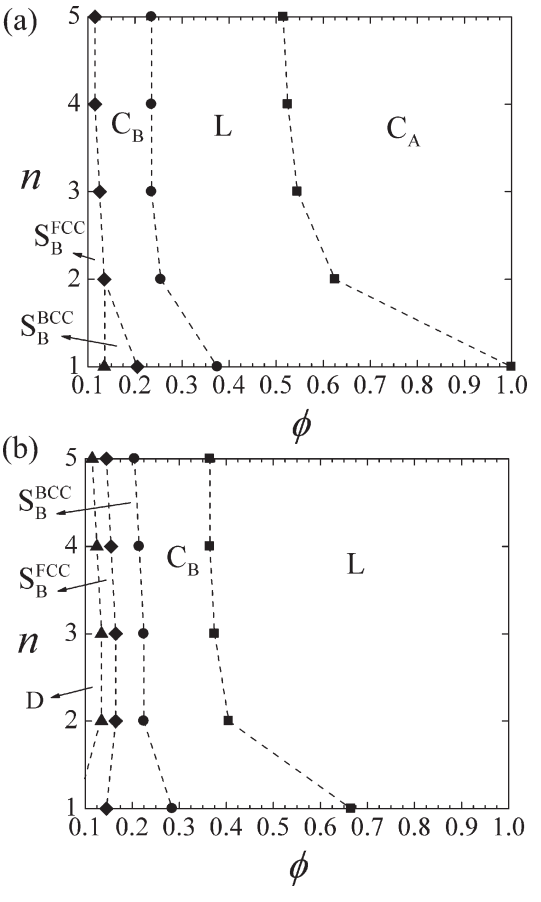

Figure 11. Two-dimensional phase maps in terms of ϕ and n for AB_n star copolymer solutions with $f =$ (a) 0.4 and (b) 0.6, $N = 150$, $\chi_{AB}N = 40$, $\chi_{AS} = 0.4$, and $\chi_{BS} = 0.7$.

Figure 5 ($n = 2$). In a further comparison of the phase boundary between each spherical order as a function of n, we find that the ordered S_A^{A15} region does not change significantly with ϕ and n, indicating that even when cutting the B component into more arms, the formed polygonal interfaces seem to saturate at this level of segregation. However, the stability of S_A^{FCC} near the ODT is greatly enhanced by suppressing the S_A^{BCC} region with an increase in the molecular asymmetry (i.e., n). This can be rationalized by considering that at a fixed value of $f = 0.25$ and the same chain length, when the number of B-arms n increases from 1 to 4, the composition of each B-arm decreases from 0.75 to 0.19. To clarify, these A-formed spheres when $n = 1-2$ are the normal ones with thicker corona layers, which are likely to pack into BCC array; while they become inverted with thinner corona layers when n increases to 4−5 and thus tend to adopt a more dense packing of FCC. If we choose a copolymer with longer A blocks (i.e., $f > 0.5$) in the presence of a B-selective solvent so that the A-formed spheres even when $n = 1-2$ are inverted, it is reasonable that the effect of varying n on the stability of FCC packing, as we have observed in the case of smaller f, disappears. For example, in Figure 10b, we plot the phase map as a function of n and ϕ for an AB_n copolymer with $f = 0.6$ and $N = 150$ at $\chi_{AB}N$ equal to 40 in the presence of a B-selective solvent by setting $\chi_{BS} = 0.4$ and $\chi_{AS} = 0.75$. Each ordered region of L, C_A^{HEX}, S_A^{A15}, and S_A^{FCC} remains almost unchanged with n and ϕ. Finally, we examine how the resultant phase behavior of AB_n miktoarm star copolymer in the presence of one A-selective solvent is influenced with n. Parts a and b of Figure 11 display the corresponding phase map for $f = 0.4$ and 0.6, respectively, and the same $N = 150$, $\chi_{AB}N = 40$, $\chi_{AS} = 0.4$, and $\chi_{BS} = 0.7$. When the copolymer varies from a linear to a miktoarm architecture, since the multi-B arms prefer less to be confined within the minor domains, we observe a significantly large region of the C_A^{HEX} and/or L, and thus only a small region of the B-formed cylinders and spheres. When increasing the number of B arms n, we observe similar phase transition behavior induced by solvent amount and solvent selectivity. However, increasing the number of B-arms n has a similar effect on the enhancement of the stability of the ordered phases, where the B-arms remain on the matrix domains. Thus, we observe that the C_A^{HEX} region slightly expands with n in Figure 11a.

IV. Conclusions

We have employed the Fourier space implementation of self-consistent mean-field (SCMF) theory to examine the phase behavior of AB_n miktoarm star copolymers in the presence of a solvent. In particular, we focus on the effects of solvent selectivity, copolymer volume fraction ϕ, A composition f, and molecular asymmetry (in our case, the number of B-arms per molecule). Generally speaking, the significant effects associated with the addition of one solvent on the AB linear diblock copolymers, as it is reported in literatures, have also been observed on the AB_n miktoarm star copolymers.

When the solvent is selective for the multi-B arms, a series of transition from the equilibrium phase in the melt into the A-formed spheres occurs upon dilution. This is analogous to decreasing the composition f in the melt case. Three packing arrays of A-formed spheres, A15, BCC, and FCC, are possible. If $f < 0.5$ so that these A-formed spheres are the normal ones, they tend to adopt the A15 and then BCC ordering before entering into the disordered region. When f increases to >0.5 so that the

A-formed spheres become inverted, a more dense packing of FCC is quite possible in addition to A15 and BCC. Similar to the AB linear diblock solutions, FCC is more favored than BCC upon increasing the solvent amount and/or solvent selectivity. Moreover, we find that when more AB_n chains aggregate to form cylinders or micelles upon increasing the solvent selectivity, a greater degree of the interfacial distortion from a round into the polygonal shape is often accompanied in order to relax the stretching penalty for the B arms on the outside domains. Hence, we observe a transition of BCC/FCC → A15 with increasing the solvent selectivity, and a significantly enlarged region of S_A^{A15} and C_A^{HEX}.

On the other hand, in the A-solvent case, a series of transition into the B-formed spheres is induced upon dilution. Since the multi-B arms experience more lateral crowding than the linear A block and thus prefer less to be confined within the minor domains, we observe a narrow region of the B-formed cylinders and spheres. Furthermore, because of the tension of the highly stretched B within the inner domains, the AB interface tends to preserve a more spherical shape; thus we do not observe any stable region of the A15 phase, but only BCC and FCC for the B-formed spheres.

Finally, based on the fact that increasing the number of B-arms n enables the B component preferable to stay on the matrix domains, the stability of the A-formed cylinders and spheres is enhanced with increasing n. Moreover, when a B-selective solvent is added to AB_n with shorter A blocks, since the A-formed spheres become more inverted with increasing n, we observe a significantly enlarged region of the S_A^{FCC} by suppressing the S_A^{BCC}.

Acknowledgment. This work was supported by the National Science Council of the Republic of China through Grant NSC 97-2628-E-002-001-MY3.

References and Notes

(1) Hadjichristidis, N.; Pispas, S.; Floudas, G. *Block Copolymers: Synthetic Strategies, Physical Properties, and Applications*; Wiley: New York, 2003.
(2) Edens, M. W.; Whitmarsh, R. H. In *Developments in Block Copolymer Science and Technology*; Hamley, I. W., Ed.; Wiley: New York, 2004.
(3) Pochan, D. J.; Gido, S. P.; Pispas, S.; Mays, J. W.; Ryan, A. J.; Fairclough, J. P. A.; Hamley, I. W.; Terrill, N. J. *Macromolecules* **1996**, *29*, 5091.
(4) Floudas, G.; Pispas, S.; Hadjichristidis, N.; Pakula, T.; Erukhimovich, I. *Macromolecules* **1996**, *29*, 4142.
(5) Tselikas, Y.; Iatrou, H.; Hadjichristidis, N.; Liang, K. S.; Mohanty, K.; Lohse, D. J. *J. Chem. Phys.* **1996**, *105*, 2456.
(6) Lee, C.; Gido, S. P.; Pitsikalis, M.; Mays, J. W.; Tan, N. B.; Trevino, S. F.; Hadjichristidis, N. *Macromolecules* **1997**, *30*, 3732.
(7) Hadjichristidis, N. *J. Polym. Sci. A: Polym. Chem.* **1999**, *37*, 857.
(8) Yang, L.; Hong, S.; Gido, S. P.; Velis, G.; Hadjichristidis, N. *Macromolecules* **2001**, *34*, 9069.
(9) Mavroudis, A.; Avgeropoulos, A.; Hadjichristidis, N.; Thomas, E. L.; Lohse, D. J. *Chem. Mater.* **2003**, *15*, 1976.
(10) Olvera de la Cruz, M.; Sanchez, I. C. *Macromolecules* **1986**, *19*, 2501.
(11) Milner, S. T. *Macromolecules* **1994**, *27*, 2333.
(12) Olmsted, P. D.; Milner, S. T. *Macromolecules* **1998**, *31*, 4011.
(13) Grason, G. M.; DiDonna, B. A.; Kamien, R. D. *Phys. Rev. Lett.* **2003**, *91*, 058304.
(14) Grason, G. M.; Kamien, R. D. *Macromolecules* **2004**, *37*, 7371.
(15) Grason, G. M. *Phys. Rep.* **2006**, *433*, 1.
(16) Huang, C. I.; Yu, H. T. *Polymer* **2007**, *48*, 4537.
(17) Voronoi, G. *J. Reine Angew. Math.* **1908**, *134*, 198.
(18) Stachurski, Z. H. *Polymer* **2003**, *44*, 6059.
(19) Balagurusamy, V. S. K.; Ungar, G.; Percec, V.; Johansson, G. *J. Am. Chem. Soc.* **1997**, *119*, 1539.
(20) Hudson, S. D.; Jung, H. T.; Percec, V.; Cho, W. D.; Johansson, G.; Ungar, G.; Balagurusamy, V. S. K. *Science* **1997**, *278*, 449.
(21) Percec, V.; Rudick, J. G.; Peterca, M.; Yurchenko, M. E.; Smidrkal, J.; Heiney, P. A. *Chem.—Eur. J.* **2008**, *14*, 3355.
(22) Vargas, R.; Mariani, P.; Gulik, A.; Luzzati, V. *J. Mol. Biol.* **1992**, *225*, 137.
(23) Luzzati, V.; Vargas, R.; Mariani, P.; Gulik, A.; Delacroix, H. *J. Mol. Biol.* **1993**, *229*, 540.
(24) Clerc, M. *J. Phys. II* **1996**, *6*, 961.
(25) Imai, M.; Yoshida, I.; Iwaki, T.; Nakaya, K. *J. Chem. Phys.* **2005**, *122*, 044906.
(26) Svensson, A.; Norrman, J.; Piculell, L. *J. Phys. Chem. B* **2006**, *110*, 10332.
(27) Sakamoto, S.; Shimojima, A.; Miyasaka, K.; Ruan, J.; Terasaki, O.; Kuroda, K. *J. Am. Chem. Soc.* **2009**, *131*, 9634.
(28) Matsen, M. W.; Schick, M. *Phys. Rev. Lett.* **1994**, *72*, 2660.
(29) Grason, G. M.; Kamien, R. D. *Phys. Rev. E* **2005**, *71*, 051801.
(30) Huang, C. I.; Hsueh, H. Y. *Polymer* **2006**, *47*, 6843.
(31) Huang, C. I.; Lodge, T. P. *Macromolecules* **1998**, *31*, 3556.
(32) Henry, N. F. M.; Lonsdale, K., Eds; *International Tables for X-ray Crystallography*; Kynoch: Birmingham, U.K., 1969.
(33) Dormidontova, E. E.; Lodge, T. P. *Macromolecules* **2001**, *34*, 9143.
(34) Wang, J.; Wang, Z. G.; Yang, Y. *Macromolecules* **2005**, *38*, 1979.
(35) Grason, G. M. *J. Chem. Phys.* **2007**, *126*, 114904.